CAMBRIDGE
UNIVERSITY PRESS

Metamaterial based stepped microstrip line fed quad-band dual-sense circularly polarized slot antenna for wireless applications

Pradeep Hattihalli Shankaraiah[1,2] (iD), Neelawar Shekar Vittal Shet[1] and Krishnamoorthy Kandasamy[1]

[1]Department of Electronics and Communication Engineering, National Institute of Technology Karnataka, Mangalore, Karnataka, India and [2]Department of Electronics and Communication Engineering, Siddaganga Institute of Technology, Tumakuru, Karnataka, India

Abstract

This research proposes a low-complexity, low-profile square-shaped quad-band dual-sense circularly polarized (CP) perturbed slot antenna with stepped microstrip feed for C-band radar and satellite applications. The proposed antenna is characterized by characteristic mode analysis. The proposed design has a square-shaped slot with diagonally opposite symmetric rectangular corner extensions. Multiband resonance is achieved by exciting the split ring resonator (SRR), cross strips and annular ring structure using the stepped microstrip line-fed slot radiator. The slot antenna and a metallic ring resonate at 1.64 and 8.2 GHz, respectively, showing left-hand circular polarization response, whereas the SRR and cross strips resonate at 3.6 and 6.6 GHz, respectively, exhibiting right-hand circular polarization radiation at these resonance bands. Hence, the proposed design shows quad-band performance with dual-sense CP behavior. Furthermore, the proposed antenna allows for independent tuning of polarization sense at resonance frequencies. The proposed design uses a low-cost FR-4 material as a substrate of dimensions $60 \times 60 \times 1.6$ mm^3. The experimentally measured results are in close agreement with the simulated performance parameters of the prototype.

Introduction

Antennas play a vital role in wireless communication systems. Using multiple antennas increases the circuit size, design complexity, and system cost. So, there is an enduring challenge for antenna designers to develop miniaturized, multiband, and cost-effective antennas. A single antenna with a multiband feature is suitable for wireless communication applications like multiple-input–multiple-output communication, cognitive radio, etc.

Many linearly polarized antennas with dual-band [1], triple-band [2] characteristics exist in the literature. Circularly polarized (CP) antenna designs [3, 4] for wireless devices have more benefits compared to linearly polarized ones due to their better multipath propagation characteristics. CP antennas with dual-band [5] and triple-band[6] characteristics have the same sense of polarization at the resonance bands. Moreover, antenna designs with a multiband operation with dual-sense CP behavior are an additional advantage for polarization diversity in wireless communication because the two antennas need not be spaced $\lambda/2$ apart and further overcome polarization mismatch problems.

Antenna designs reported in references [7] and [8] exhibit dual-band and triple-band operations, respectively, with dual-sense polarization behavior. The above antenna designs have a restriction of less than four bands of operation.

Many quad-band antennas [9–12] with linear polarization characteristics are found in the literature. Also, there exists quad-band, dual polarized antennas with single CP band [13, 14], dual-band CP [15], and triple-band CP [16] designs. In these designs, the number of CP resonances are limited.

There also exists quad-band CP antenna designs with a single-sense of polarization characteristics. These include capacitive-coupled stacked patch antenna [17], frequency-selective surface (FSS) backed patch antenna [18], and series-fed circular slit microstrip array antenna [19].

The following antenna designs exhibit quad-band, dual-sense CP response.

In reference [20], a novel design of a stacked annular patch antenna with probe-feed achieves dual-sense CP radiation by employing a stripline quadrature phase feed network.

Communication [21] represents an open square-ring structured radiator, an inverted V-shaped parasitic strip and a rhombic-type slot to achieve quad-band operation.

An aperture-coupled cylindrical dielectric resonator antenna (DRA) is reported in reference [22], which exhibits dual-sense CP characteristics due to the tilted L-shaped slot and L-shaped perturbations in the circular aperture.

Asymmetric co-planar waveguide (CPW)-fed quad-band monopole antenna consisting of an annular ring radiator is proposed in reference [23], which shows CP resonances due to asymmetric ground plane, a cross-shaped slit, a rectangular open loop and a tuning stub in the feed structure.

The above dual-sense CP antenna designs lack independent tuning of the polarization sense. The additional feature of tuning the CP sense gives further flexibility in antenna design and hence, ease of implementation for wireless communication applications.

Recently, self-quadruplexing CP substrate-integrated waveguide (SIW) based slot radiator is reported in reference [24]. This work has four unequal-length T-shaped slots etched out on a square SIW cavity, excited by four microstrip lines to generate CP waves. This design shows dual-sense CP with independent tuning of the polarization sense. The axial ratio bandwidths (ARBWs) of 1.22%, 1.15%, 1.46%, and 1.33% are achieved.

Metamaterials (MTM) are artificially engineered materials, whose first approach was the design and implementation of the split ring resonators (SRR) [25, 26]. Integration with antennas, SRRs exhibit desirable features like miniaturization, circular polarization, and multiband operation.

In reference [27], corner truncated slot with outer ring connected SRRs produce dual-band, dual-sense CP characteristics with independent tuning of polarization sense.

Square-shaped slot antenna with SRR and metallic strips loaded is realized in reference [28], to achieve triband, dual-sense CP behavior with flexibility to tune polarization sense independently.

Designing an antenna with low-profile, compact with simple feed mechanism to achieve quad bands of operation with independent circular polarization sense tunability and diversity for wireless communication applications is a challenge.

Circular polarization diversity enhances the performance of antenna systems by providing flexibility and robustness against environmental changes, improving signal quality, and ensuring reliable communication across various applications like satellite communication and mobile networks etc.

The proposed design represents a novel approach to address the challenges of modern wireless communications by enhancing polarization diversity, improving bandwidth (BW), and maintaining compactness, making it suitable for C-band radar and satellite communication applications.

In this communication, a MTM-inspired quad-band, dual-sense CP characterized by a square-shaped planar slot antenna is proposed. The perturbed slot radiator is loaded with the MTM unit cell, cross strips, and a metallic annular ring structure to achieve multiband operation. It is designed to exhibit CP bands at 1.64, 3.6, 6.6, and 8.2 GHz. The impedance BWs of 15.38%, 9.18%, 54.20%, and ARBWs of 4.25%, 0.83%, 13.49%, and 0.48%, and peak gains of 1.72 dBic, 2.40 dBic, 5.24 dBic, and 6.53 dBic are achieved at resonance bands. The proposed design provides wide impedance and ARBWs, high CP isolaton and peak gain values and flexibility to change the CP orientation compared to other works.

The key contributions of the proposed design are as follows:

1. By embedding SRR, cross strips, and annular metallic ring in the perturbed slot structure, four pairs of orthogonal polarizations with opposite rotations are established.

2. Design flexibility to tune the polarization sense independently at the resonance bands.
3. Low profile, compact size, high gain, better CP isolation, and ease of fabrication compared to other works.
4. Equivalent circuit analysis to validate the $|S_{11}|$ characteristics.
5. Characteristic mode analysis (CMA) to study the orthogonal modes responsible for CP generation.

The rest of the article is divided into the following sections: The quad-band antenna geometry and its evolution steps and the mechanism of CP generation of the proposed design are described in the section "Antenna design and working principle." CMA, parametric study, circuit equivalent model and surface current distributions at resonance bands are discussed in the section "Antenna analysis." The section "Experimental results and discussion" gives the comparison of simulated and measured values of performance parameters, followed by the conclusion in the section "Conclusion."

Antenna design and working principle

Antenna geometry

The proposed design is a CP quad-band slot antenna using a FR-4 dielectric material (relative permittivity $\varepsilon_r = 4.4$, substrate thickness $h = 1.6$ mm, and loss tangent $\tan\delta = 0.025$) of size 60×60 mm^2. A square-shaped slot is etched on the top side of the substrate to resonate at its fundamental resonant mode. Further, to produce CP waves at the slot resonance frequency, diagonally opposite symmetric rectangular corner extensions are added to the slot. The slot radiator is suitably excited by a stepped microstrip feed line printed at the bottom of the dielectric material. The stepped feed line has impedance variation of 50 Ω (for width $W_f = 2.9$ mm, length $L_f = 4$ mm), 68 Ω (for $W_{f1} = 1.6$ mm, $L_{f1} = 25.3$ mm), and 82.8 Ω (for $W_{f2} = 1$ mm, $L_{f2} = 11$ mm). A perturbed slot with a side length of 40.5 mm, is designed to resonate at 1.64 GHz. The MTM SRR unit cell is placed near the bottom edge of the slot, below the substrate, at distances $d_1 = 10.75$ mm and $d_2 = 21.2$ mm with respect to the reference axes(xy-plane). Furthermore, the slot is loaded with asymmetric cross strips coupled to a metallic annular ring. The perturbed slot loaded with the SRR, cross strips, and a metallic ring structure generates quad resonances with CP characteristics. Figure 1 illustrates the proposed quad-band antenna geometric configuration. The final optimized dimensional values are given in Table 1.

SRR unit cell

The geometry of the proposed SRR is depicted in Fig. 1(c). It comprises of square-shaped concentric rings with split gaps at opposite edges. The unit cell dimensions are shown in Table1. The SRR unit cell can be circuit modelled as a parallel inductance (L) and capacitance (C) resonance network with its frequency of operation given by references [29, 30].

In order to confirm the MTM property of the proposed unit cell, the effective medium parameters of the proposed resonator are obtained from the scattering parameters [31]. The parametric retrieval method for the SRR is based on Nicholson-Ross-Weir method [32].SRR is characterized using the waveguide setup [29] in CST Microwave studio as shown in Fig. 2(a)

This is performed by placing the proposed SRR printed on a FR-4 substrate inside a waveguide setup and an electromagnetic wave
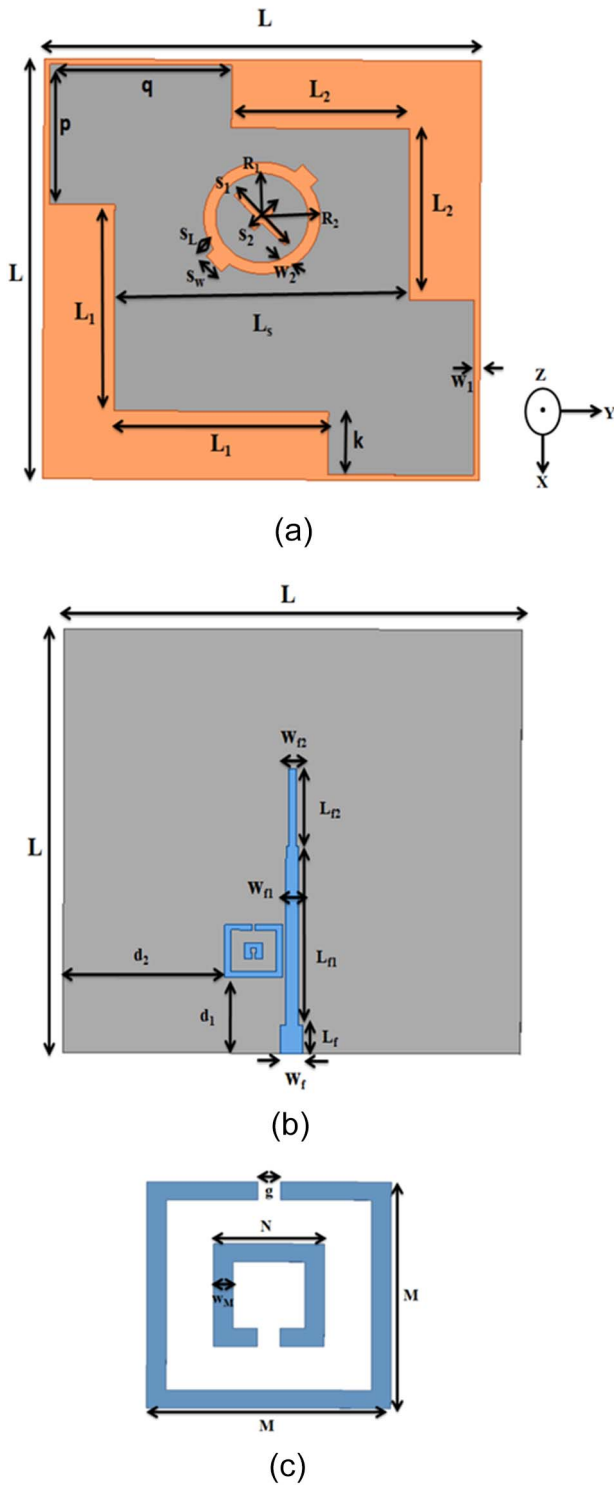
Figure 1. Proposed quad-band antenna geometric configuration: (a) Top view, (b) Bottom view, (c) SRR unit cell geometry.

Table 1. Final optimized physical parameter values of the proposed design

Parameters	Values(in mm)		
		g	0.38
L	60	W_1	0.75
L_S	40.5	W_2	1
L_1	29.5	R_1	6.4
L_2	24.5	R_2	8
p	20	S_L	0.5
q	25	S_W	3
k	9	W_f	2.9
S_1	10	L_f	4
S_2	4	W_{f1}	1.6
M	7.5	L_{f1}	25.3
N	2.3	W_{f2}	1
W_M	0.8	L_{f2}	11

The simulated S_{11} and S_{21} values are used for the extraction of effective medium parameters. The extracted real and imaginary parts of permittivity are shown in Fig. 2(c). It is inferred that the negative permittivity is observed for the frequency 3.58 GHz. At this resonance frequency, the negative permittivity leads to strong interactions with electromagnetic waves, effectively creating a stop band. Thus, it is confirmed that the proposed unit cell is a epsilon-negative (ENG) MTM-inspired structure.

The proposed unit cell has contributed to the notch at 3.58 GHz in the return loss characteristics of the proposed slot radiator. The resonator exhibits negative values of permittivity in the frequency range of 3.11–4.17 GHz, which overlaps with the resonance band 3.46–3.78 GHz of the proposed radiator. Thereby, implanting SRR with optimized parameters in the proposed slot radiator, contributes a new resonance frequency of 3.58 GHz for achieving quad-band antenna.

Quad-band resonance

This segment describes the proposed radiator's operation principle at different evolution stages. Figure 3 depicts the realization of quad-band design with the help of different antenna configurations. The simulated $|S_{11}|$ performance and AR curves for different antenna prototypes are illustrated in Fig. 4.

Ant. A: The conventional square-shaped slot radiator is excited by microstrip feed line to resonate at its fundamental transverse electric (TE_{10}) mode with resonance frequency [33] of,

$$f_r = \frac{c}{2L_s}\sqrt{\frac{2}{1+\epsilon_r}} \tag{1}$$

where ε_r denotes the relative permittivity of the substrate material, and L_s is the length of the slot. This configuration has the large value of AR (>40 dB). Figure 4(a) depicts this conventional prototype resonates at 1.63 GHz.

Ant. B: The perturbation introduced in the form of symmetric rectangular extensions at the diagonally opposite corners of the slot generates a CP band at 1.63 GHz, as illustrated in Fig. 4(b).

The diagonal extension of the corners creates asymmetry in the slot geometry, which significantly influences the current distribution and modifies the effective impedance of the slot structure.
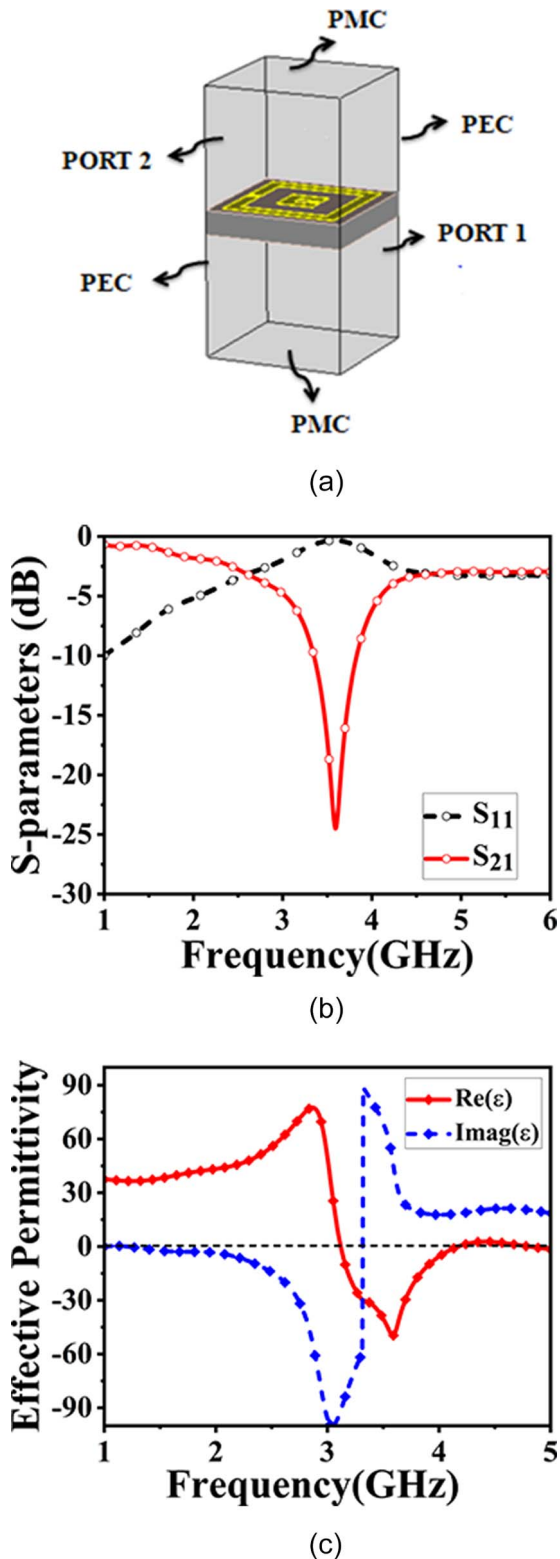
is passed through one port and reflection (S_{11}) and transmission coefficients (S_{21}) are measured on the other port.

The simulation based scattering parameters representing stop band phenomenon of the SRR at a frequency of 3.58 GHz is depicted in Fig. 2(b). The SRR exhibits stop band characteristics at 3.58 GHz, indicated by strong attenuation ($S_{21} \approx -25$ dB) and high reflection($S_{11} \approx 0$ dB).

(a)

(b)

(c)

Figure 2. SRR unit cell characterization: (a) Waveguide setup, (b) Reflection and transmission behavior, (c) Negative permittivity characteristics of the proposed unit cell.

Extending the slot corners introduces higher order modes TE_{20}, TE_{30}, and so on, that resonate at frequencies above the fundamental mode and are characterized by additional current paths within the slot structure. Careful design of the slot and the feed
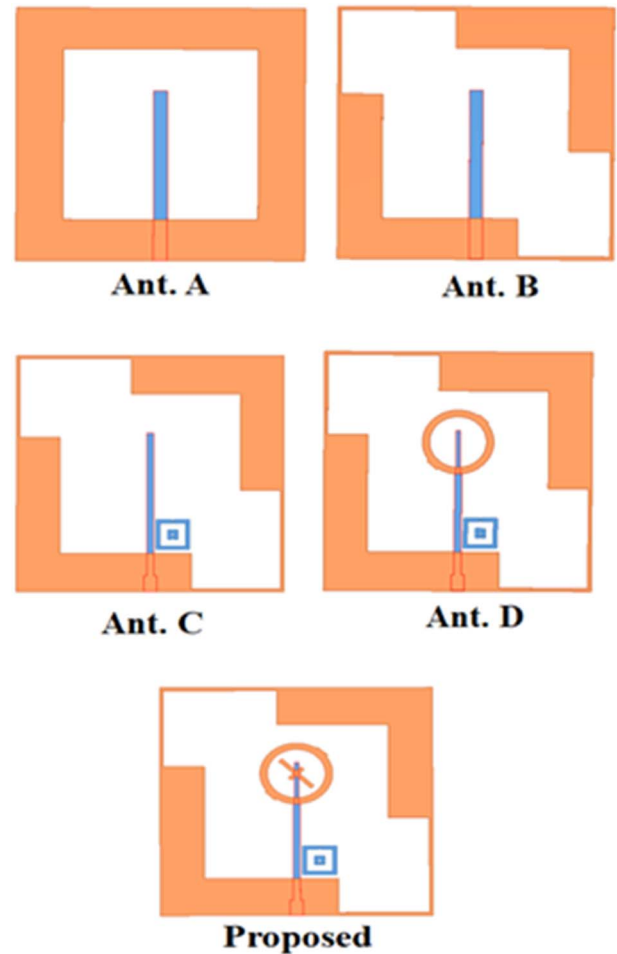

Figure 3. Emergence of the proposed quad-band antenna.
Proposed: Further, the loading of asymmetric cross strips within a metallic annular ring can excite two orthogonal modes that can combine to produce CP. The asymmetry in the cross strips introduces quadrature phase difference between the orthogonal modes. The interaction between the annular ring and the cross strips enhances the coupling between the excited modes. This leads to CP radiation at 8.17 GHz.

system ensures efficient excitation of orthogonal degenerate modes TE_{10} and TE_{01} with quadrature phase relationship. This combination produces a rotating electric (E) field vector that characterizes circular polarization.

Ant. C: The SRR is placed below the substrate material at lower edge of the slot radiator. With this configuration, apart from fundamental mode, higher-order resonances are generated at 3.58 and 8 GHz due to the placement of SRR as a result of electromagnetic coupling with the fields from the slot structure. As the resonator supports current loops, and these currents circulate, they generate higher-order resonances characterized by different current distributions. Fine tuning the SRR geometry as well as its proper orientation and position relative to the slot results in two pairs of orthogonal degenerate modes such as TE_{10} and TE_{01}, TE_{20} and TE_{02} modes, corresponding to each CP band.

Ant. D: Embedding annular metallic ring within the perturbed slot further alters the current distribution and the E field in the slot, thereby affecting the radiation characteristics of the slot radiator. Optimizing the dimensions and placement of the annular ring in relation to the slot ensures better coupling between them which
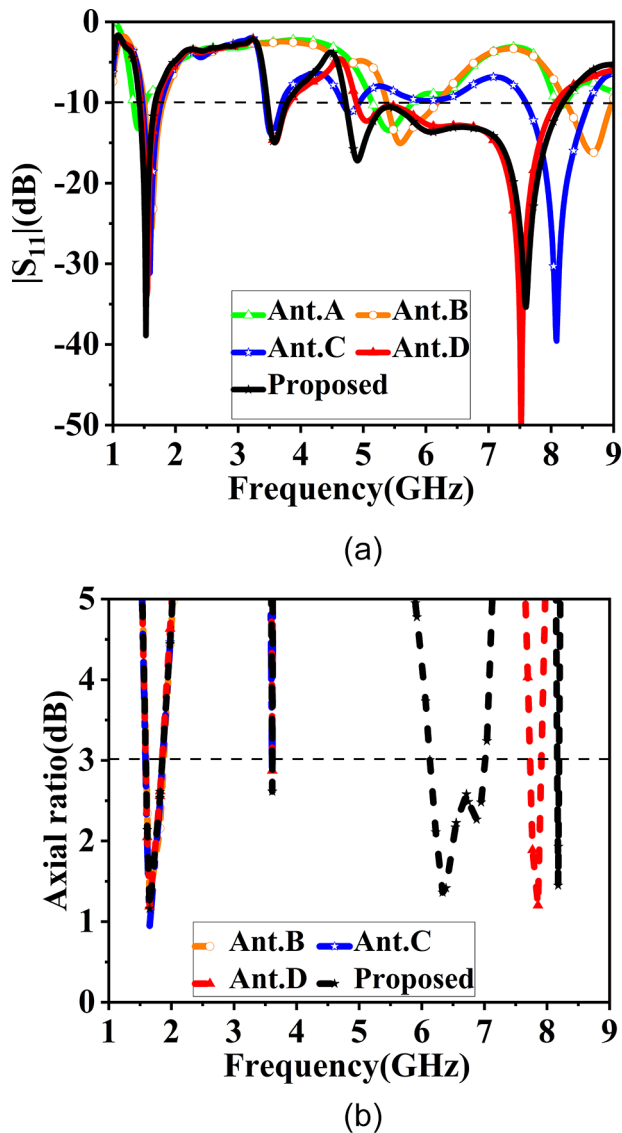
Figure 4. Antenna evolution: (a) $|S_{11}|$ performance and (b) AR curves.

contributes to new resonances, particularly at higher frequencies. As a result, the higher order resonances of perturbed slot (Ant. B) are combined to give wide impedance band. Stubs loading to the annular ring creates asymmetry in the structure, eventually resulting in two orthogonal degenerate modes TE_{30} and TE_{03} for CP resonance at 7.85 GHz.

The longer strip length is chosen based on the guided wavelength given by reference [33],

$$\lambda_g = \frac{300}{f_r, GHz \sqrt{\varepsilon_{eff}}} \qquad (2)$$

where the effective dielectric constant ε_{eff} is determined by:

$$\varepsilon_{\text{eff}} = \frac{\varepsilon_r + 1}{2} + \frac{\varepsilon_r - 1}{2\sqrt{1 + 12\left(\frac{h}{W_f}\right)}} \qquad (3)$$

W_f denotes the feed line width, and h is the thickness of the substrate material. The longer strip length is approximately considered to be half of the guide wavelength (λ_g) at the resonant frequency.

Table 2. Performance comparison of different prototypes and the proposed slot radiator

Prototypes	No. of CP bands	IBW (GHz, %)	ARBW (GHz, %)	Modifications in the geometry
Ant. A	Nil	1.32–1.52, 14 5.14–5.77, 11.54	——	Conventional slot
Ant. B	1	1.50–1.79, 17.62 5.37–6.19, 14.18 8.23–8.97, 8.60	1.60–1.68, 4.87	Perturbed slot having diagonal corner extensions
Ant. C	2	1.47–1.76, 17.95 3.44–3.70, 7.28 7.59–8.60, **12.47**	1.59–1.67, 4.90 3.56–3.6, 1.11	Implanting ENG resonator cell
Ant. D	3	1.44–1.72, 17.72 3.47–3.81, 9.34 4.88–8.07, 49.26	1.59–1.67, 4.90 3.56–3.6, 1.11 7.80–7.85, **0.63**	Embedding annular metallic ring structure in the slot
Proposed	4	1.42–1.67, 16.18 3.46–3.78, 8.83 4.72–8.20, **53.86**	1.59–1.67, 4.90 3.56–3.6, 1.11 6.12–7.0, **13.55** 8.15–8.20, 0.61	Placement of asymmetric cross strips within annular ring

The stepped microstrip feed can provide better impedance matching over a wider frequency range. The different widths and lengths of the steps can create controlled phase shifts in the signal. This is crucial for exciting multiple orthogonal modes that are essential for generating CP bands in the above configurations. It further improves the performance of slot radiator in terms of BW, gain, and radiation efficiency.

The simulated results in terms of IBW and ARBW of different prototypes and the proposed slot configuration are summarized in Table 2.

The simulation results in Table 2 indicate that no CP resonance is contributed by the prototype Ant. A. The perturbed slot configuration in the prototype Ant. B gives rise to single CP band. Embedding MTM cell in the perturbed slot radiator results in dual CP bands for the prototype Ant. C. Further, comparing the performances of Ant. C and the proposed design, there is large enhancement of IBW of the third resonance band from 12.47% to 53.86% resulting two additional CP bands. Comparing the prototype Ant. D and the proposed design, there is large BW improvement of the third axial ratio band from 0.63% to 13.55% resulting in quad-band dual-sense CP antenna.

Furthermore, the four resonance bands of operation of the proposed design can be noticed from the simulation results of E field distributions depicted in Fig. 5. The lowest resonance band at 1.63 GHz is contributed due to the perturbed slot structure shown in Fig. 5(a).
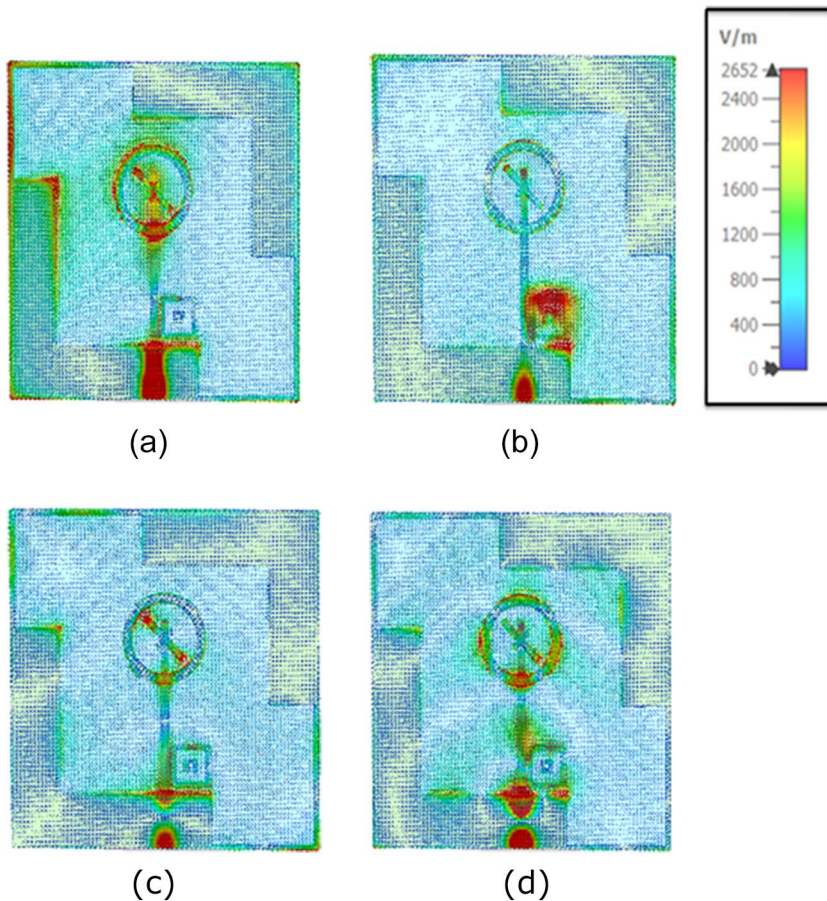
Figure 5. Comparison of resonance bands through simulated E-field behavior at:(a) 1.63 GHz, (b) 3.58 GHz, (c) 6.56 GHz, and (d) 8.17 GHz.

The SRR is designed to generate a CP band at 3.58 GHz shown in Fig. 5(b). The loading of cross strips and annular metallic ring results in resonance bands at 6.56 and 8.17 GHz, respectively. This is illustrated in Fig. 5(c) and Fig. 5(d), respectively.

CP mechanism

The two diagonally opposite symmetric rectangular corner extensions of the slot radiator generate the field components which are orthogonal in nature with phase quadrature, thus, giving rise to CP waves at the slot-resonant frequency. By altering the position of extensions to other diagonal opposite corners, the sense of polarization can be changed.

The slot resonance along with the excitation of the SRR cell results in CP behavior at the second resonance band. This resembles like the magnetic dipole-loop combination that generates field components orthogonal in nature [34]. By changing the orientation of the SRR by 180°, the CP sense can be altered.

The asymmetry due to the unequal length of cross strips results in orthogonal components of E-fields. The generation of CP waves can be realized by the degenerate modes. The polarization sense can be reversed due to a change in the orientation of the strips by 90°.

The diametric loading of rectangular stubs to the annular metallic ring creates asymmetry, thereby producing the orthogonal field components with 90° phase difference for CP response. The polarization sense can be tuned independently by rotating the metallic ring by 90°.
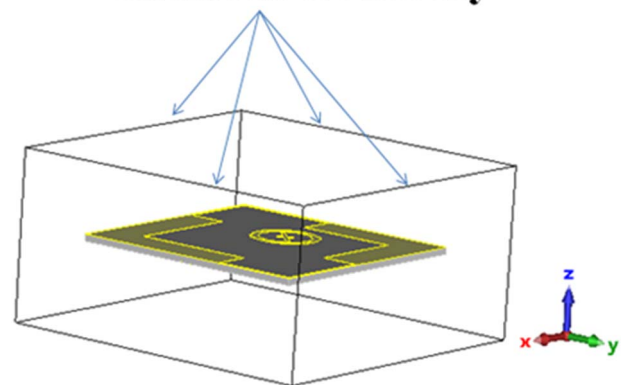

Figure 6. Open radiation boundary set up for CM analysis.

Antenna analysis

Characteristic mode analysis

CMA is a powerful technique used in antenna design and electromagnetic analysis. It gives physical insight to understand the intrinsic behavior of antenna structures and their modes of radiation. CMA focuses on identifying the natural resonant modes that can exist within the structure that contribute to desired characteristics like radiation patterns and polarization. In reference
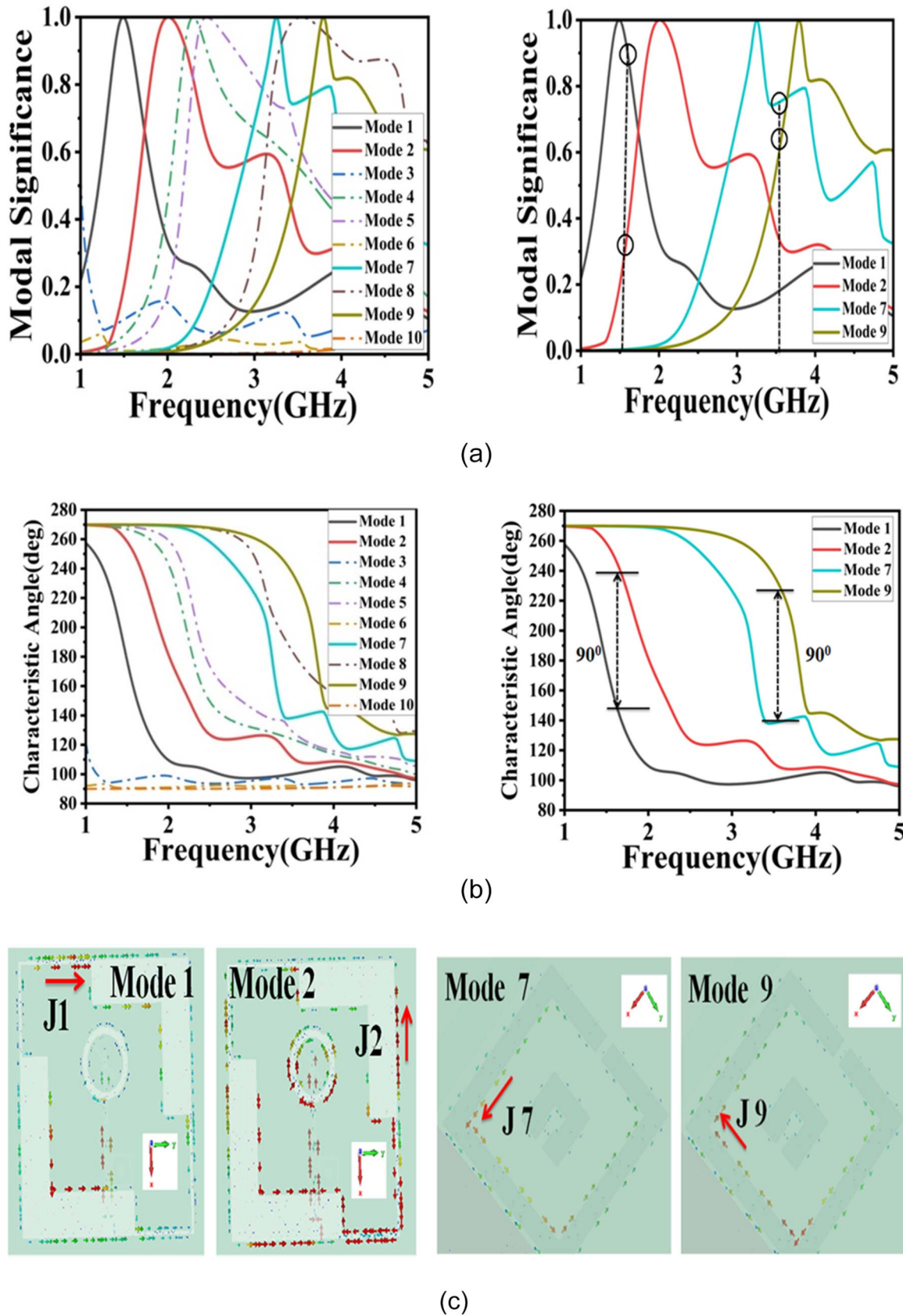
(a)

(b)

(c)

Figure 7. Simulated CMA performance at 1.59 GHz(CP band-1) and 3.56 GHz(CP band-2): (a) MS, (b) CA, (c) Modal current distribution, and (d) Modal radiation pattern.
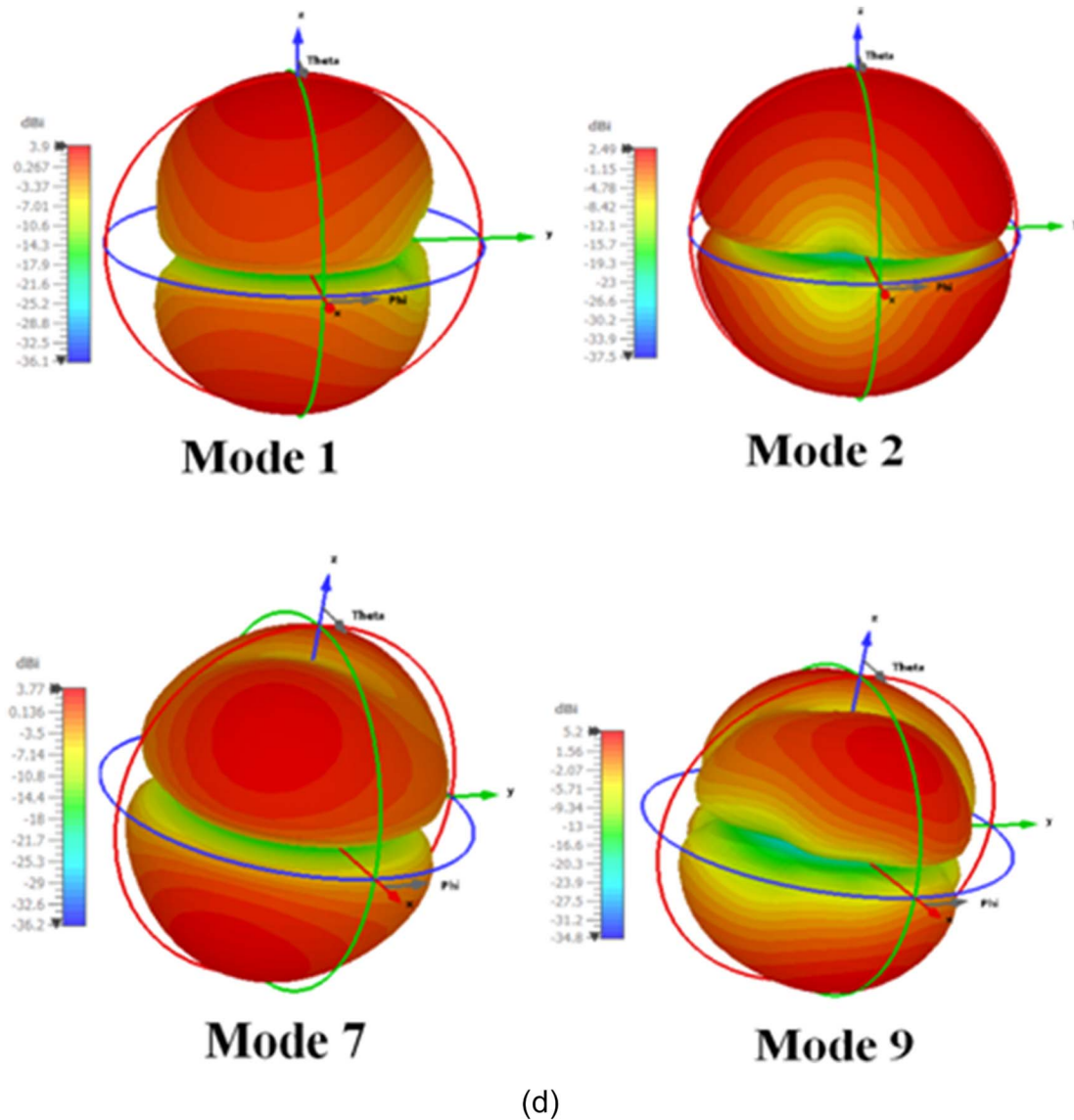
Mode 1

Mode 2

Mode 7

Mode 9

(d)

Figure 7. (Continued.)

[35], the theory of characteristic modes (CM) was proposed to characterize the surface current and radiating field on perfectly conducting bodies. In CM theory, the CM of a conducting surface are determined using eigen value equation $XJ_n = \lambda_n RJ_n$, where λ_n represents the eigen value of the nth CM and J_n is the characteristic current of the nth mode. Eigenvalues play a crucial role in determining the resonance behavior of each mode. The key parameters which effectively determine the mode behavior are modal significance (MS = $1/(1 + \lambda_n)$) and characteristic angle (CA = $180° - \lambda_n$). MS is a measure of the effectiveness of a particular mode in contributing to the radiation pattern of an antenna. CA offers valuable insights into the orientation and phase relationships of the modes in an antenna design.

In this section, the CMA performance of the proposed CP slot radiator is explored. It is analyzed using a method of moment-based CMA tool in CST Microwave Studio. The Fig. 6 shows the open radiation boundary set up for the analysis. In the proposed design, CMA is performed to determine the CM responsible for CP radiation. Figure 7 depicts simulated CMA performance in terms of MS, CA, modal current distribution, and modal radiation pattern at 1.59 and 3.56 GHz.

The MS of Mode1(J1) is 0.90 and Mode 2 (J2) is 0.36, indicating J1 is more significant than J2 with the phase difference of the CA between them is 90° at 1.59 GHz. Further, the surface currents J1 and J2 travel orthogonally along the inner and outer edge of the slot structure, respectively and the far-field radiation patterns are of symmetric-lobe radiation, resulting in the CP behaviour at 1.59 GHz.

The MS of Mode 7 (J7) and Mode 9 (J9) are 0.75 and 0.63 respectively, highlighting J7 is more dominant than J9 in contributing to the radiation performance of the antenna at 3.56 GHz with 90° phase difference between them. Furthermore, the modal currents J7 and J9 are normal to each other along the outer ring of the SRR and the modal field patterns are bidirectional in nature and exhibit CP radiation at 3.56 GHz.
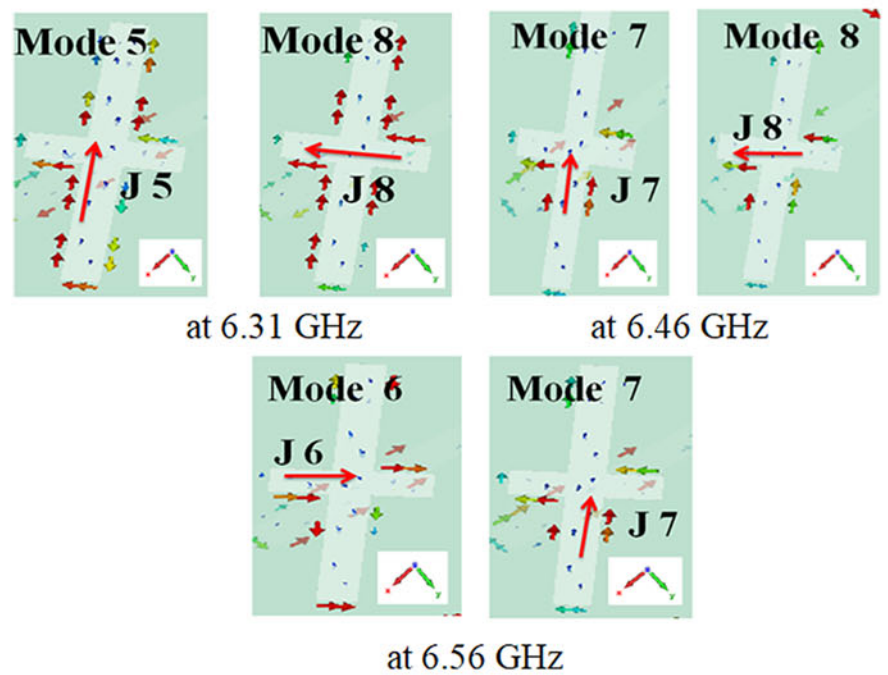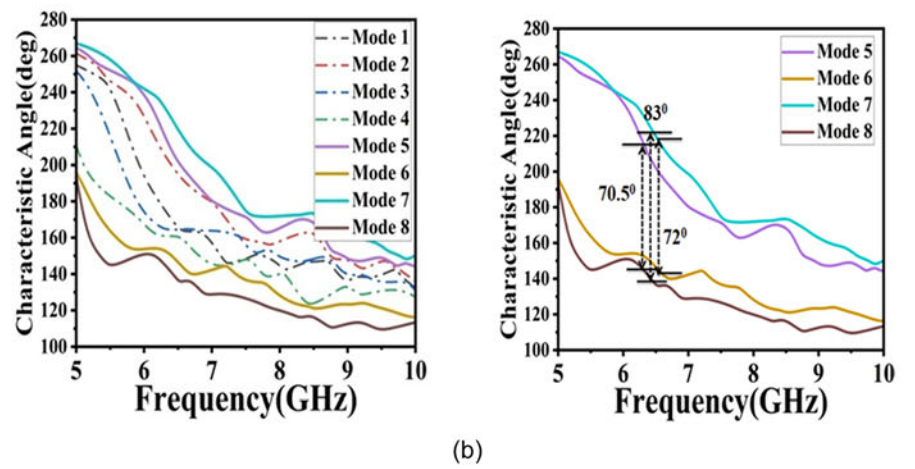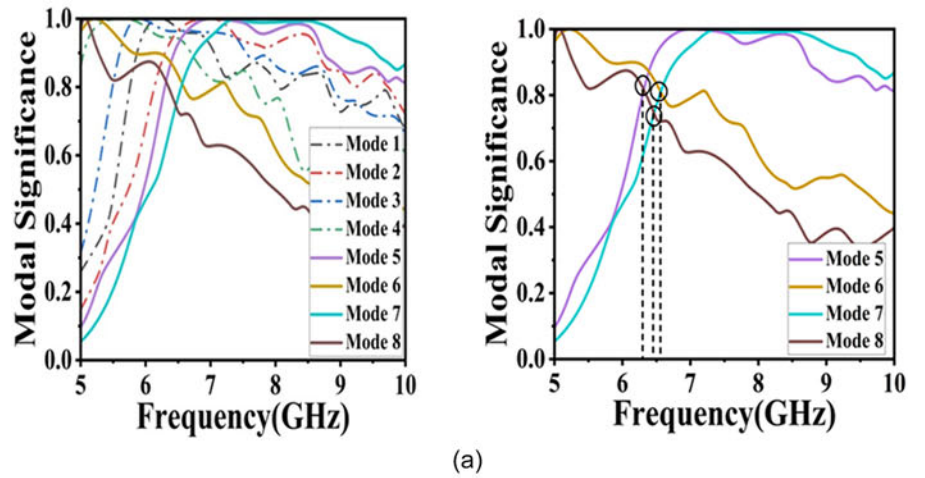
Figure 8. Simulated CMA performance at 6.31, 6.46, and 6.56 GHz(CP band-3): (a) MS, (b) CA, (c) Modal current distribution, and (d) Modal radiation pattern.
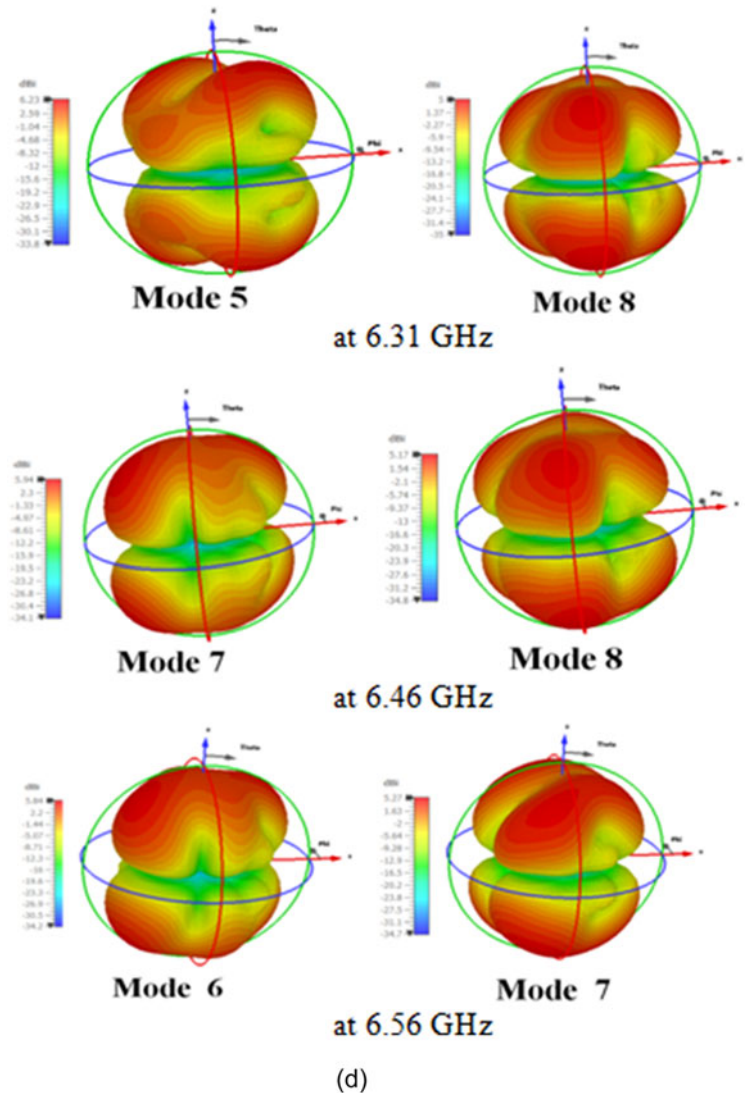
Figure 8. (Continued.)

Figure 8 depicts simulated CMA performance in terms of MS, CA, modal current distribution, and modal radiation pattern at 6.31, 6.46, and 6.56 GHz.

Additionally, it is found that the following mode pairs: (J5, J8), (J7, J8), and (J6, J7) have equal MS values of 0.81, 0.74, and 0.80 with 70.5°, 83°, and 72° phase differences, respectively at higher frequencies 6.31, 6.46, and 6.56 GHz. Even though the phase shift is less than 90° between two modes before feed excitation, CP can be achieved satisfactorily after feed excitation [36]. Figure 8(c) depicts that surface currents are dominant at two perpendicular directions along the asymmetric cross strips and modes are well radiated in bore-sight direction as shown in Fig. 8(d), resulting in CP radiation.

Figure 9 depicts simulated CMA performance in terms of MS, CA, modal current distribution, and modal radiation pattern at 8.16 GHz.

The modes J8 and J15 have MS values of 0.47 and 0.86 respectively, with 90° phase difference and exhibit broadside radiation at 8.16 GHz. The surface currents are orthogonal in nature along the annular ring structure. J8 and J15 are the pair of orthogonal modes which are responsible for circular polarization.

This analysis reveals that the above mentioned orthogonal modes have the potential to radiate CP waves at the resonance bands of the proposed design. Therefore, the CMA results are consistent with the results of the full-wave simulation.

Surface current analysis

To obtain a good physical insight of the operation of the proposed antenna, this section illustrates CP characteristics of the quad-band design by observing the simulated surface current flow at resonance bands on the slot structure, the SRR, cross strips and a metallic annular ring at phases $\omega t = 0°$ and $\omega t = 90°$. From the Fig. 10, it is observed that the current distributions are positive z-directed on the xy-plane. The current density vectors are considered along the directions of maximum current density and J_{res} represents the resultant current density vector. In Fig. 10(a), it is seen that for phase $\omega t = 0°$, the resultant current density J_{res} is controlled by vertical components J_1 and J_2. For 90° phase, the horizontal components J_1 and J_2 contribute for the resultant current density. Thus, it is observed that as phase progresses, the resultant current density vector rotates clock wise direction to give left-hand circular polarization (LHCP) radiation at 1.63 GHz.
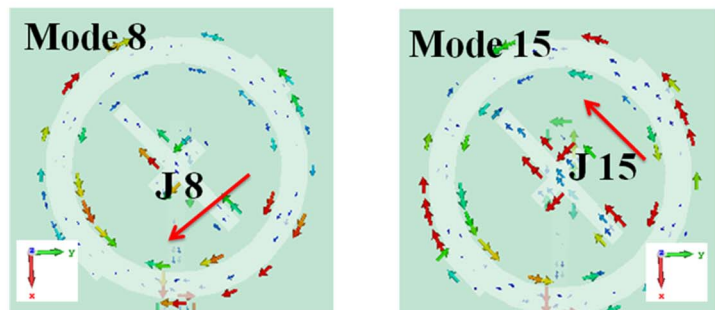
At the second CP resonance, for the 0° phase, the amplitude of resultant current density is mainly controlled by the components J_1
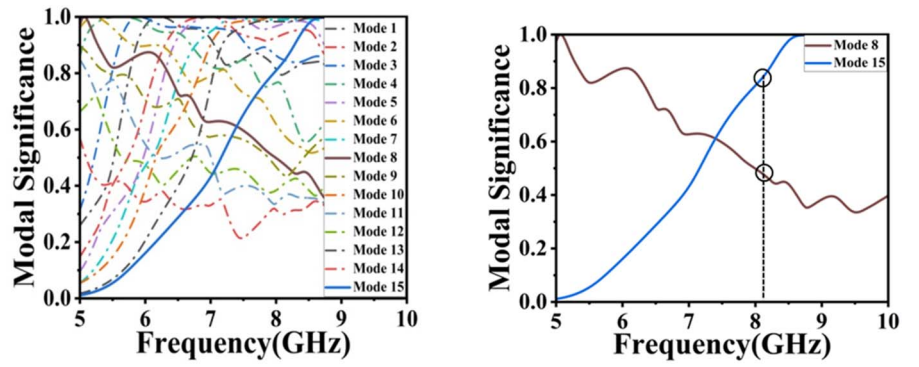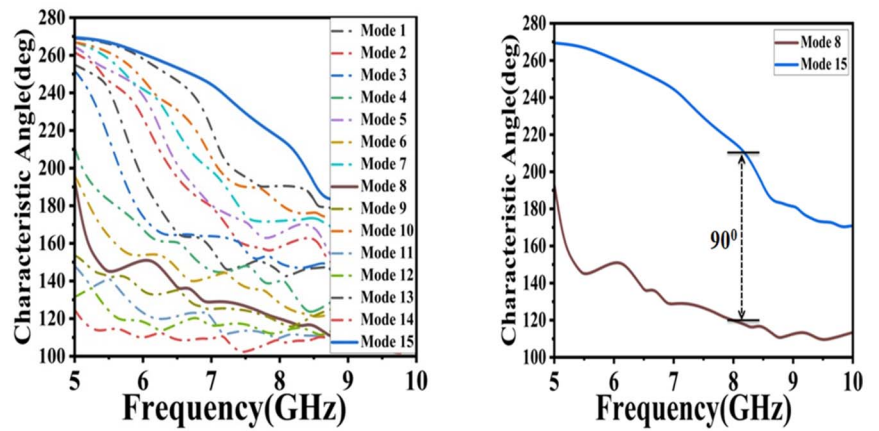
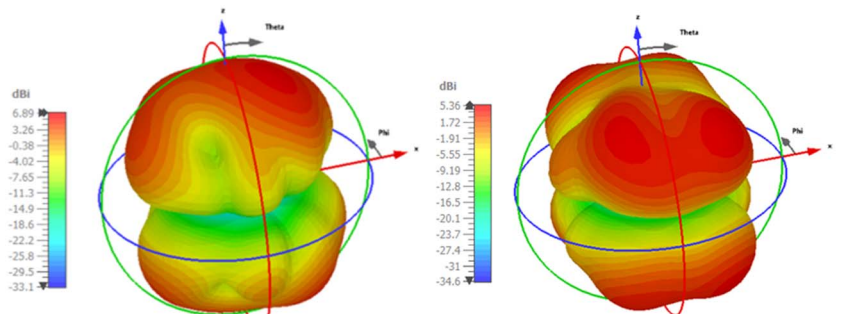**Figure 9.** Simulated CMA performance at 8.16 GHz(CP Band-4): (a) MS, (b) CA, (c) Modal current distribution, and (d) Modal radiation pattern.
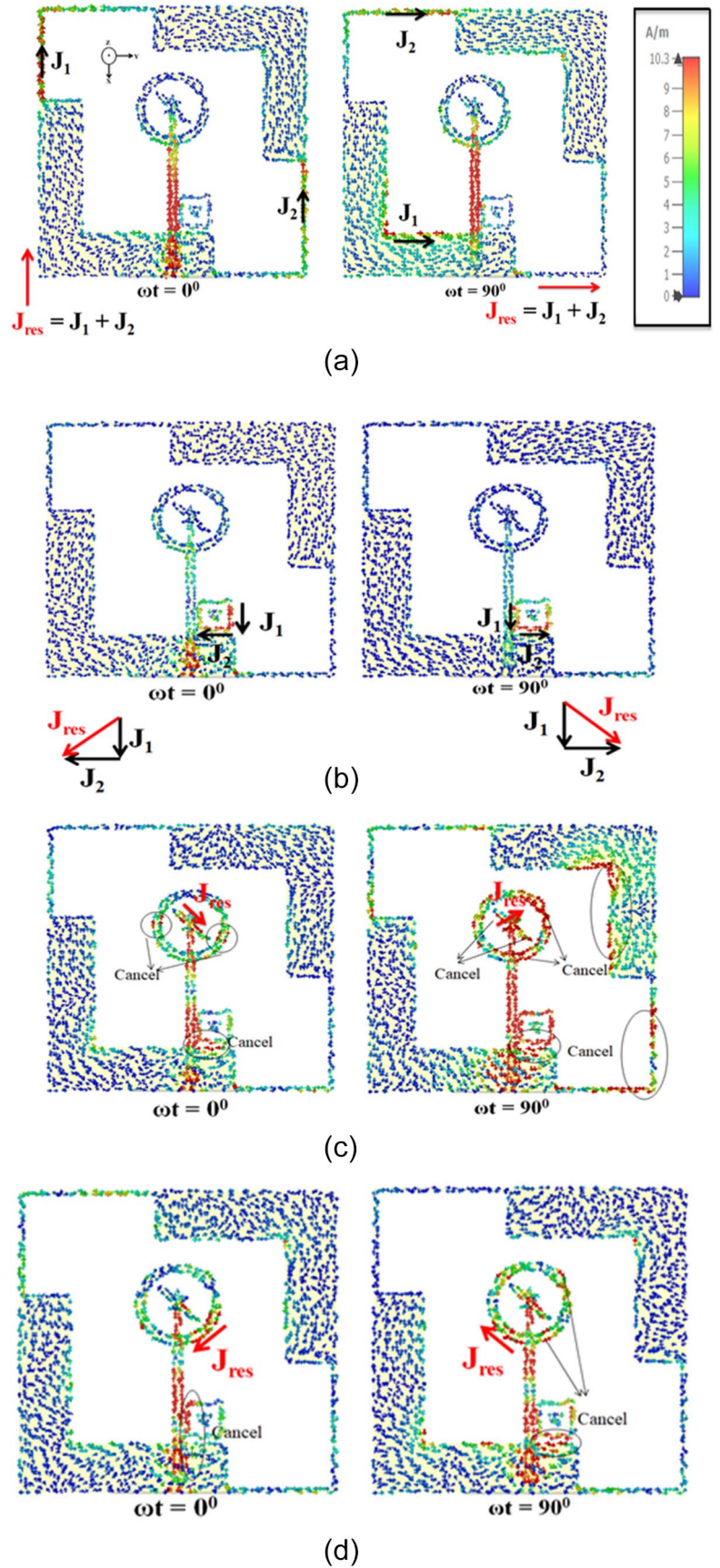
Figure 10. Surface current flow at resonance bands:(a) 1.63 GHz, (b) 3.58 GHz, (c) 6.56 GHz, and (d) 8.17 GHz.
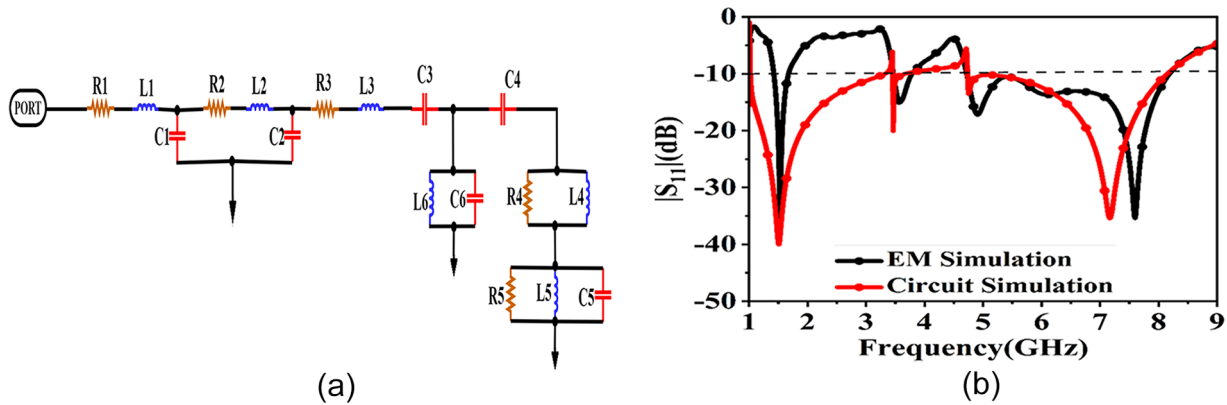
Figure 11. (a) Circuit equivalent model, (b) Comparison of reflection coefficient plots.

and J_2, and oriented along $-135°$ direction. As the phase advances to $90°$, the resultant J_{res} rotates to $-45°$ direction in anticlock wise direction to radiate RHCP waves at 3.58 GHz as illustrated in Fig. 10(b).

For the resonances 6.56 and 8.17 GHz, the proposed antenna radiates RHCP and LHCP waves, respectively as the phase progresses from $0°$ to $90°$ and also accounting for the cancelation effect of oppositely flowing current components in some directions as depicted in Fig. 10(c) and (d).

A reversal in the current direction is expected with a change in the position of the corner extensions and the rotation of a metallic ring by $90°$. Hence, in this case, the antenna emits RHCP waves at resonances 1.63 and 8.17 GHz. Also, it is observed that due to a change in the orientation of the cross strips by $90°$ and the MTM cell by $180°$, a reversal in the direction of the current vector is noticed. Hence, LHCP behavior is observed at frequencies 3.58 and 6.56 GHz. Hence, the proposed design has a dual-sense CP response with the independent tuning of polarization sense at each of the resonance frequencies.

Circuit equivalent analysis

The circuit simulation is carried out using Advanced Design System simulation software. The circuit equivalent transmission line representation of the proposed quad-band radiator is shown in Fig. 11(a). The stepped microstrip feed line is represented by a circuit comprised of lumped components $R1$, $L1$, $C1$, $R2$, $L2$, $C2$, $R3$, and $L3$. The capacitances $C3$ and $C4$ represent the slot coupling. The parallel combination of discrete elements $L6$ and $C6$ indicate the circuit equivalent of a SRR. Further, the loading of an annular metallic ring and cross strips in a perturbed slot structure gives rise to a quad-band response. These strips coupling to metallic ring are represented by parallel resistance, inductance, and capacitance (RLC) and resistance and inductance (RL) resonant circuits in a series connection. Figure 11(b) depicts the S-parameter behavior of the proposed design obtained using electromagnetic (EM) simulation and circuit model. The return loss performance due to the circuit behavior is in close agreement with EM simulation.

The optimized values of lumped elements due to circuit simulation are $R1 = 2.1\ \Omega$, $L1 = 1.626$ nH, $C1 = 0.407$ pF, $R2 = 53.20\ \Omega$, $L2 = 1.85$ nH, $C2 = 3.987$ pF, $R3 = 0.30\ \Omega$, $L3 = 2.80$ nH, $R4 = 50$ KΩ, $L4 = 2.678$ nH, $R5 = 1\Omega$, $L5 = 0.1$ nH, $C5 = 0.1$ pF, $L6 = 4.989$ nH, $C6 = 3.409$ pF, $C3 = 0.555$ pF, $C4 = 0.969$ pF.

Parametric analysis

The parametric variation of key dimensions is conducted to analyze the effects on $|S_{11}|$ performance and ARBW of the resonance bands of the antenna. This analysis involves variation of a single parameter value at a time, keeping rest of the other parameters constant at a final optimized value. The significant parameters of this design are cross strip length (S_1), annular ring radius (R_1), feed line width (W_{f1}), and feed line length (L_{f2}).

A. Cross strip length(S_1):

Figure 12(a) shows the $|S_{11}|$ performance and AR curves for the variation of strip length. The impedance BW of the upper wideband improves slightly with the increase in strip length. Due to the increase of strip length, the ARBW of the third CP band increases greatly. Further, results in quad-band CP antenna.

B. Annular ring radius (R_1):

Figure 12(b) depicts the simulation results of $|S_{11}|$ plots and AR curves for varying values of annular ring radius. As the ring radius increases, the upper wideband impedance BW increases slightly and the ARBW of the third CP band widens. For $R_1 = 5.6$ and 6 mm, 6.4 mm, the proposed antenna exhibits triband and quad-band CP performances, respectively.

C. Feed line width (W_{f1}):

Figure 12(c) illustrates the simulated $|S_{11}|$ behavior and AR plots for the varying values of feed line width. There is no much variation in the BW performance of the proposed design. However, the occurrence of a number of CP resonances varies due to the variation in feed line width. For an optimized value of $W_{f1} = 1.6$ mm, this antenna design shows quad-band CP performance.

D. Feed line length (L_{f2}):

Figure 12(d) shows the reflection coefficient magnitudes and AR performance for feed line length variation. As the feed line length increases, there is a shift in the upper wideband toward the lower frequency side. For the decreased value of $L_{f2} = 10$ mm and for the increased value of $L_{f2} = 12$ mm, the third CP band gets split up and becomes narrower, respectively. For an optimized value of $L_{f2} = 11$ mm, the design results in a quad-band CP antenna.
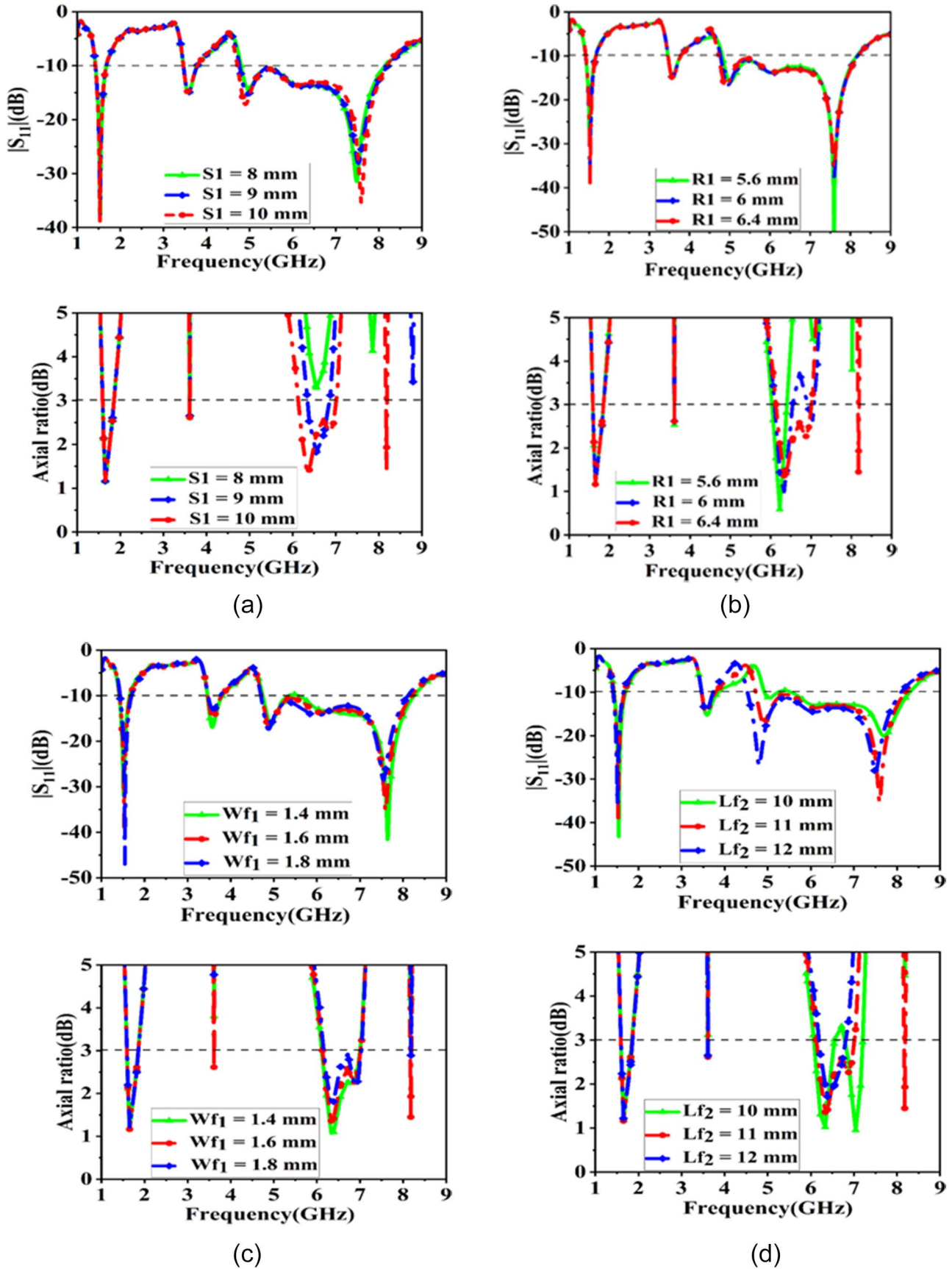
Figure 12. Simulated $|S_{11}|$ and AR curves for parametric variation of: (a) S_1, (b) R_1, (c) W_{f1}, and (d) L_{f2}.

Experimental results and discussion

The simulation was performed using the CST Microwave Studio software, and later, the final optimized quad-band square slot design was fabricated using the S103 LPKF PCB prototyping machine. The experimentally measured performance of the fabricated antenna is validated with the simulation results.

Figure 13 shows the fabricated antenna prototype and setup for antenna measurement. The Agilent N9918A Vector Network Analyzer was used for S-parameter measurement. The antenna measured values agree well with the simulated results. The small differences between the two results are due to measurement tolerances and fabrication errors.

Figure 14 illustrates the $|S_{11}|$ plots and axial ratio curves obtained from the measurement and simulation of the proposed quad-band design.

The measured $|S_{11}| < -10$-dB BWs obtained for different resonant frequencies were 15.38% (range from 1.44 to 1.68 GHz), 9.18% (range from 3.53 to 3.87 GHz), 54.20% (range from 4.72 to

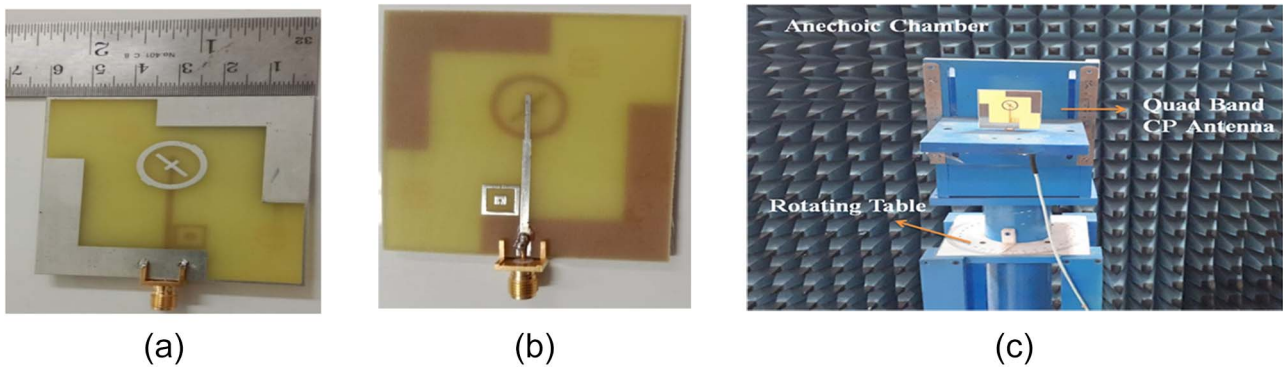**Figure 13.** Fabricated antenna prototype: Top sight (b) Bottom sight; (c) Setup for antenna measurement.
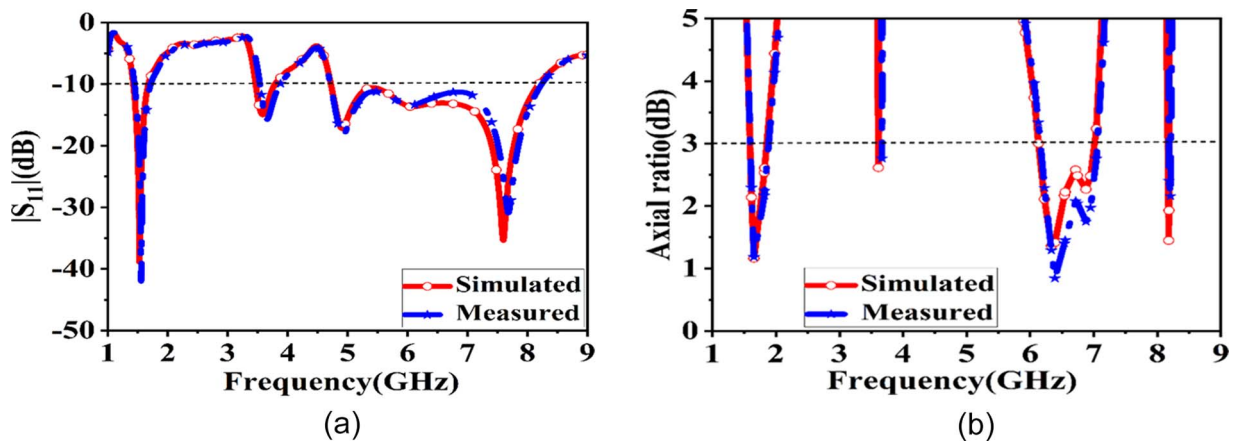

Figure 14. Simulated and measured results: (a) S-parameter values, (b) AR curves.
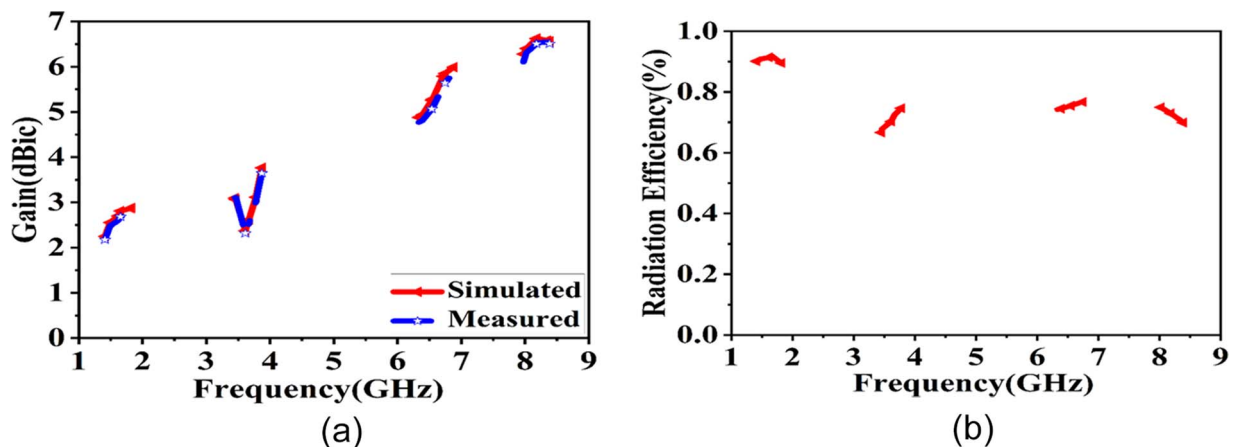

Figure 15. Simulated and experimentally measured results: (a) Peak gain,(b) Simulated Efficiency values.
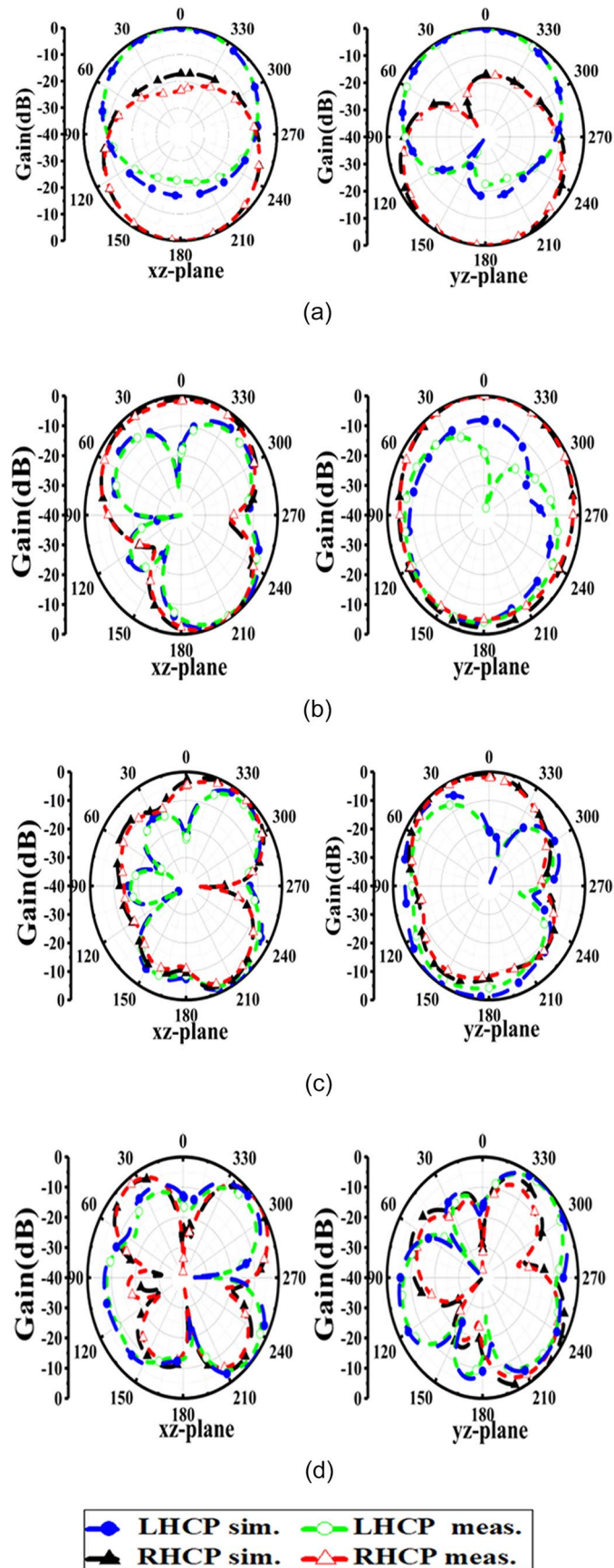
Figure 16. Comparison of radiation plots at: (a) 1.64 GHz, (b) 3.6 GHz, (c) 6.6 GHz, and (d) 8.2 GHz.

Table 3. Comparative analysis of this work with existing quad-band circularly polarized designs found in the literature

Ref. No.	Antenna type & feed	Dimensions(mm³)	Resonance bands(GHz)	IBW (%)	ARBW (%)	Peak gain (dBic)	CP sense	Pol. sense tunability	Min. RHCP to LHCP isolation (dB)
[17]	Stacked patch, coaxial probe feed	18.83 × 16.4 × 7.56	5.14, 5.59, 6.30, 7.72	55.46	0.98, 4.27, 0.88, 1.35	——-	Single	No	18
[18]	Patch antenna with FSS, microstrip line feed	133.2 × 133.2 × 32.54	2.4, 3.5, 5.3, 5.8	14.84, 80.7	5.4, 8.3, 3.7, 2.9	5.95, 6.92, 6.37, 6.07	Single	No	9
[19]	Circular microstrip array antenna, microstrip line feeds	41 × 41 × 2	2.5, 3.5, 3.8, 5.2	33.85, 50.73	16.26, 12.52, 8.22, 13.82	2.51, 4.62, 4.32, 2.76	Single	No	13
[20]	Stacked patch, quadrature phase feed network	70 × 12 × 5.7	1.26, 1.57, 1.61, 2.49	0.61, 0.40, 0.64, 1.57	For all bands <1	2.14, 2.74, 3.42, 5.43	Dual	No	12
[21]	Planar monopole, microstrip line feed	75 × 65 × 1.52	2.5, 2.9, 3.5, 5.4	83.9	7.3, 9, 3.7, 7.1	2.5, 2.9, 3.4, 2.7	Dual	No	9
[22]	DRA, aperture feed	120 × 120 × 29.6	1.1, 1.5, 2.3, 2.6	21.1, 12.82, 27.06, 7.54	11.65, 7.64, 7.01, 7.1	———	Dual	No	15
[23]	Planar annular ring, CPW feed	35 × 30 × 1.6	5.63, 7.69, 9.91, 12.09	10.02, 4.96	2.13, 8.46, 12.11, 1.32	———	Dual	No	17
[24]	SIW cavity-backed slot, microstrip line feeds	31.5 × 31.5 × 0.787	8.85, 10.4, 11.4, 12.23	5.27, 2.99, 2.83, 4.42	1.22, 1.15, 1.46, 1.33	6.5, 6.1, 5.25, 6.35	Dual	Yes	21.5
Proposed	MTM-inspired planar slot, microstrip line feed	60 × 60 × 1.6	1.64, 3.6, 6.6, 8.2	15.38, 9.18, 54.20	4.25, 0.83, 13.49, 0.48	2.72, 2.40, 5.24, 6.53	Dual	Yes	18

Abbreviation: BW, bandwidth.

8.23 GHz), whereas the simulated $|S_{11}| < -10$-dB BWs obtained were 16.18% (range from 1.42 to 1.67 GHz), 8.83% (range from 3.46 to 3.78 GHz), 53.86%(range from 4.72 to 8.20 GHz).

The measured values of 3-dB ARBWs obtained for different resonance bands were 4.25% (range from 1.61 to 1.68 GHz), 0.83% (range from 3.59 to 3.62 GHz), 13.49% (range from 6.15 to 7.04 GHz) and 0.48% (range from 8.17 to 8.21 GHz), whereas the simulated 3-dB ARBWs obtained were 4.90% (range from 1.59 to 1.67 GHz), 1.11% (range from 3.56 to 3.6 GHz), 13.55% (range from 6.12 to 7.01 GHz) and 0.61% (range from 8.15 to 8.20 GHz).

The measured peak gains of 2.72 dBic, 2.40 dBic, 5.24 dBic, and 6.53 dBic, whereas the simulated peak gains of 2.78 dBic, 2.45 dBic, 5.45 dBic, and 6.62 dBic and simulated radiation efficiency of 91.68%, 69.83%, 75.55%, and 73.13% were obtained at resonance frequencies. Figure 15 depicts the measured and simulated plots of CP gain and simulated efficiency values of the quad-band radiator.

The radiation performance of the proposed design were measured using a near-field anechoic chamber. Figure 16 reveals the radiation plots of the quad-band CP design in two principal planes (xz and yz) at the resonance bands.

The proposed radiator emits LHCP waves at the resonance bands 1.64 and 8.2 GHz and RHCP radiation at 3.6 and 6.6 GHz, in the positive z-direction.

From the plots, it is evident that the radiation plots have bidirectional patterns and are in reasonable agreement with the simulated and measured values of co-pol and cross-pol levels in quad bands. For the resonance frequencies 1.64 and 8.2 GHz, LHCP is stronger than RHCP by approximately 18 dB, whereas for the resonances 3.6 and 6.6 GHz, the RHCP to LHCP isolation is greater than 20 dB, in the boresight direction ($\theta = 0°$).

To discuss the novelty with respect to previously reported works, a comparative analysis is made in Table 3. This table compares the proposed design with other quad-band CP antennas in the literature in terms of size, BWs, gain and flexibility to tune the polarization sense independently. Most of the reported quad-band CP designs have large profile, either multiple or complex feed

system, either less BWs or gain and lack of flexibility to tune the polarization sense independently.The designs [17, 18] have large profile with single-sense circular polarization. Multiple feed lines are employed in reference [19], with single-sense CP characteristics. The large profile with complex feed structure and less BWs are realized in reference [20]. The designs reported in references [21–23] have either large profile, lesser gain values or no independent tuning of polarization sense. The proposed antenna can be better compared with reference [24] as they have similar features like compact planar slot structure with dual-sense CP and provision for independent tuning of polarization sense. But, the design in reference [24] has four ports and shows lesser impedance and ARBWs. Although the proposed antenna schemes in references [18, 19, 21] achieved wide IBW and ARBW, they suffer from either less peak gain or less CP isolation, either bulkiness or multiple feeds, and either single CP sense or lack of independent tuning of CP sense.

Therefore, the proposed radiator is the best trade-off, while still accounting for the aspect of size and performance parameters that include IBW, ARBW, peak gain, CP isolation, and independent tuning of CP sense, thus proving it to be the most viable potential candidate in practical wireless communication applications requiring circular polarization sense tunability and diversity.

Conclusion

A planar quad-band perturbed square slot antenna for CP radiation is presented in this article. Multiband resonances are achieved by the corner extended slot radiator loaded with cross strips, a metallic annular ring and the SRR unit cell. The antenna exhibits measured impedance BWs of 15.38%, 9.18%, 54.20%, and measured ARBWs of 4.25%, 0.83%, 13.49% and 0.48% at the working bands. The maximum measured value of the peak gain achievable is 6.53 dBic. CMA, parametric study, equivalent circuit model and study of surface current behaviour were carried out at the resonance bands. The experimentally measured results agree well with the simulated ones. In summary, this antenna design is well suitable for modern wireless applications for quad-band CP radiation as it offers a low-profile, compact size with a dual-sense of polarization and the design flexibility to tune the polarization sense independently compared to other works.

References

1. **Liu S, Wu W and Fang DG** (2016) Single-feed dual-layer dual-band E-shaped and U-slot patch antenna for wireless communication application. *IEEE Antennas and Wireless Propagation Letters* **15**, 468–471.
2. **Paul PM, Kandasamy K and Sharawi MS** (2017) A tri-band slot antenna loaded with split ring resonators. *Microwave and Optical Technology Letters* **59**, 2638–2643.
3. **Midya M, Ghosh A and Mitra M** (2021) Meander-line-loaded circularly polarized square-slot antenna with inverted-L-shaped feed line for C-band applications. *IET Microwaves, Antennas & Propagation* **15**, 1425–1431.
4. **Ghosh A, Islam SN and Das S** (2020) A wideband compact antenna with quad-circular polarized bands in its operating regions. *International Journal of RF and Microwave Computer-Aided Engineering* **30**, e22405.
5. **Sung Y** (2021) Wideband circularly polarized antenna for dual-band operation. *Microwave and Optical Technology Letters* **63**, 286–294.
6. **Tang H, Wang K and Wu R** (2017) Compact triple-band circularly polarized monopole antenna for WLAN and WiMAX applications. *Microwave and Optical Technology Letters* **59**, 1901–1908.
7. **Rui X, Li J and Wei K** (2016) Dual-band dual-sense circularly polarised square slot antenna with simple structure. *Electronics Letters* **52**, 578–580.
8. **Kumari K, Jaiswal RK and Srivastava KV** (2020) A compact triple band circularly polarized planar antenna for wireless application. *Microwave and Optical Technology Letters* **62**, 2611–2617.
9. **Ali T, Khaleeq MM, Pathan S and Biradar RC** (2018) A multiband antenna loaded with metamaterial and slots for GPS/WLAN/WiMAX applications. *Microwave and Optical Technology Letters* **60**, 79–85.
10. **Nanda Kumar M, Yogaprasad K and Anitha VR** (2020) A quad-band Sierpenski based fractal antenna fed by co-planar waveguide. *Microwave and Optical Technology Letters* **62**, 893–898.
11. **Qian JF, Chen FC, Xiang KR and Chu QX** (2019) Resonator-loaded multi-band microstrip slot antennas with bidirectional radiation patterns. *IEEE Transactions on Antennas and Propagation* **67**, 6661–6666.
12. **Tewari N, Joshi N and Srivastava S** (2024) A compact quad-band circular cavity backed substrate integrated waveguide antenna for millimetre wave applications. *Microwave and Optical Technology Letters* **66**, e33766.
13. **Brar RS, Saurav K, Sarkar D and Srivastava KV** (2018) A quad-band dual-polarized monopole antenna for GNSS/UMTS/WLAN/WiMAX applications. *Microwave and Optical Technology Letters* **60**, 538–545.
14. **Kumar A, Deegwal JK and Sharma MM** (2018) Design of multi-polarised quad-band planar antenna with parasitic multistubs for multiband wireless communication. *IET Microwaves, Antennas & Propagation* **12**, 718–726.
15. **Darimireddy NK, Reddy RR and Prasad AM** (2018) Tri-band and quad-band dual L-slot coupled circularly polarized dielectric resonator antennas. *International Journal of RF and Microwave Computer-Aided Engineering* **28**, e21409.
16. **Badisa A, Madhav BTP, Srilatha K, Rao MC and Das S** (2022) A circularly polarized quad-band wearable textile antenna integrated with triple band AMC reflector for WBAN applications. *Progress In Electromagnetics Research C* **121**, 1–18.
17. **Singh DK, Kanaujia BK, Dwari S, Pandey GP and Kumar S** (2015) Novel quad-band circularly polarized capacitive-fed microstrip antenna for C-band applications. *Microwave and Optical Technology Letters* **57**, 2622–2628.
18. **Hoang TV, Le TT, Li QY and Park HC** (2016) Quad-band circularly polarized antenna for 2.4/5.3/5.8-GHz WLAN and 3.5-GHz WiMAX applications. *IEEE Antennas and Wireless Propagation Letters* **15**, 1032–1035.
19. **Maity B and Nayak SK** (2022) Compact quad-band cp series-fed circular slit microstrip array antenna using machine learning. *IEEE Access* **10**, 116650–116661.
20. **Li J, Shi H, Li H and Zhang A** (2014) Quad-band probe-fed stacked annular patch antenna for GNSS applications. *IEEE Antennas and Wireless Propagation Letters* **13**, 372–375.
21. **Le TT and Yun T-Y** (2019) A quad-band dual-sense circularly-polarized square-ring antenna for multi-functional wireless applications. *IEEE Access* **7**, 149634–149640.
22. **Sharma A, Das G, Gupta S and Gangwar RK** (2020) Quad-band quad-sense circularly polarized dielectric resonator antenna for GPS/CNSS/WLAN/WiMAX applications. *IEEE Antennas and Wireless Propagation Letters* **19**, 403–407.
23. **Dhara R, Yadav S, Sharma MM, Jana SK and Govil MC** (2021) A circularly polarized quad-band annular ring antenna with asymmetric ground plane using theory of characteristic modes. *Progress In Electromagnetics Research M* **100**, 51–68.
24. **Kumar K, Priya S, Dwari S and Mandal MK** (2020) Self-quadruplexing circularly polarized SIW cavity-backed slot antennas. *IEEE Transactions on Antennas and Propagation* **68**, 6419–6423.
25. **Pendry JB, Holden AJ, Robbins DJ and Stewart WJ** (1999) Magnetism from conductors and enhanced nonlinear phenomena. *IEEE Transactions on Microwave Theory & Techniques* **47**, 2075–2084.

26. **Shelby RA, Smith DR and Schultz S** (2001) Experimental verification of a negative index of refraction. *Science (New York, N.Y.)* **292**, 77–79.

27. **Kandasamy K, Majumder B, Mukherjee J and Ray KP** (2016) Dual-band circularly polarized split ring resonators loaded square slot antenna. *IEEE Transactions on Antennas and Propagation* **64**, 3640–3645.

28. **Paul PM, Kandasamy K and Sharawi MS** (2018) A triband circularly polarized strip and SRR-loaded slot antenna. *IEEE Transactions on Antennas and Propagation* **66**, 5569–5573.

29. **N. Engheta and R. W. Ziolkowski**, Eds.. (2006) *Metamaterials: Physics and Engineering Explorations*. New York, NY, USA: Wiley

30. **Ishikawa A, Tanaka T and Kawata S** (2007) Frequency dependence of the magnetic response of split-ring resonators. *Journal of the Optical Society of America B* **24**, 510–515.

31. **Smith DR, Schultz S, Markoš P and Soukoulis CM** (2002) Determination of effective permittivity and permeability of metamaterials from reflection and transmission coefficients. *Physical Review B* **65**, 5104–5109.

32. **Nicolson AM and Ross GF** (1970) Measurement of the intrinsic properties of materials by time-domain techniques. *IEEE Transactions on Instrumentation and Measurement* **19**, 377–382.

33. **Balanis CA** (2005) *Antenna Theory: Analysis and Design*. 3rd. New York, NY, USA: Wiley.

34. **Kraus JD and Marhefka RJ** (2003) *Antennas for All Applications*. 3rd. New York, NY, USA: McGraw-Hill.

35. **Harrington RF and Mautz JR** (1971) Theory of characteristic modes for conducting bodies. *IEEE Transactions on Antennas And Propagation* **19**, 622–628.

36. **Yang X, Liu Y and Gong S** (2018) Design of a wideband omnidirectional antenna with characteristic mode analysis. *IEEE Antennas and Wireless Propagation Letters* **17**, 993–997.

Pradeep Hattihalli Shankaraiah received the B.E. degree in Electronics and Communication Engineering and M.Tech degree in Digital Electronics from Visvesvaraya Technological University, Belgaum, Karnataka, India, in 2004 and 2007, respectively. He is the student member of IEEE. He is presently a Ph.D Research scholar at the Department of Electronics and Communication Engineering, National Institute of Technology Karnataka, Mangalore, India. His field of research includes antenna design, multiband antennas, metamaterial-based antennas, and reconfigurable antennas.

Neelawar Shekar Vittal Shet received the B.E. degree in Electronics and Communication Engineering from Manipal Institute of Technology, Udupi in 1984, and the M.E. degree in Communication Systems from IIT, Roorkee in 1992 and the Ph.D. degree in Electronics and Communication Engineering from NITK, Surathkal in 2011. Currently, he has been working as Professor and Head of the Department of Electronics and Communication Engineering, NITK Surathkal, Mangalore, India. His current research interests include cellular mobile communication, wireless networking, IOT and sensor networks.

Krishnamoorthy Kandasamy received the B.E. degree in Electronics and Communication Engineering from Bharathiar University, Coimbatore, India, in 2002, and the M.E. degree in Communication Systems from Anna University, Chennai, India, in 2007 and the Ph.D. degree in Electrical Engineering from IIT Bombay, Mumbai, India, in 2016. He worked as a member of technical staff in HCL Technologies, India and a Deputy Engineer, BEL, Bangalore, India. Currently, he has been working as an Associate Professor in the Department of Electronics and Communication Engineering, NITK Surathkal, Mangalore, India. His current research interests include antenna design, metamaterials, reconfigurable and multiband antenna design, microwave integrated circuits (MICs), and monolithic MICs and metasurfaces.